v

Gradient Flows and Geometric Active Contour Models

Satyanad Kichenassamy
Department of Mathematics
University of Minnesota
Minneapolis, MN 55455
email: kichenas@ima.umn.edu

Arun Kumar
Department of Aerospace Eng.
University of Minnesota
Minneapolis, MN 55455
email: arun@aem.umn.edu

Peter Olver
Department of Mathematics
University of Minnesota
Minneapolis, MN 55455
email: olver@ima.umn.edu

Allen Tannenbaum
Department of Electrical Engineering
University of Minnesota
Minneapolis, MN 55455
email: tannenba@ee.umn.edu

Anthony Yezzi, Jr.
Department of Electrical Engineering
University of Minnesota
Minneapolis, MN 55455
email: ayezzi@ee.umn.edu

September 1994

Abstract

In this note, we analyze the geometric active contour models proposed in [10, 31] from a curve evolution point of view and propose some modifications based on gradient flows relative to certain new metrics. This leads to a novel snake paradigm in which the feature of interest may be considered to lie at the bottom of a potential well. Thus the snake is attracted very naturally and efficiently to the desired feature. Moreover, we consider some 3-D active surface models based on these ideas.

Key words: Active vision, shape and object representation, object recognition, active contours, snakes, visual tracking, edge detection, segmentation, gradient flows, Riemannian metrics, geometric heat equations, curve and surface evolution.

Gradient Flows and Geometric Active Contour Models

Abstract

In this note, we analyze the geometric active contour models proposed in [10, 31] from a curve evolution point of view and propose some modifications based on gradient flows relative to certain new metrics. This leads to a novel snake paradigm in which the feature of interest may be considered to lie at the bottom of a potential well. Thus the snake is attracted very naturally and efficiently to the desired feature. Moreover, we consider some 3-D active surface models based on these ideas.

Summary

1. **Original contribution:** The contribution of this work is an active contour and surface model based on novel gradient flows, differential geometry, and curve and surface evolutions.

2. **Importance of the contribution:** The scheme we derive for the computation of deformable contours as well as our numerical routines make this type of approach ideal for segmentation, edge and curve detection, visual tracking, and shape modelling. Moreover, we believe we elucidate some underlying mathematical principles for geometric active contour models based on our gradient flow paradigm.

3. **Related works and how this work differs:** This work was strongly influenced by the geometric evolution models of Caselles *et al.* [10] and Malladi *et al.* [31]. There is an extensive literature on deformable contours references to which may be found in the book by Blake and Yuille [8]. However, in our case we derive our model from basic differential geometric principles (gradient flows relative to a Riemannian metric which depends on the given image) which leads to a new gradient term appearing in these previous models and which makes the evolution more efficient and natural.

4. **How other researchers can make use of this work:** Researchers working in active vision will have an efficient natural procedure for employing active contours to various kinds of imagery. Our scheme seems to work very well on noisy images with which other methods seem to have problems.

1 Introduction

Recently, a number of approaches have been proposed for the problem of snakes or active contours. The underlying principle in these works is based upon the utilization of deformable contours which conform to various object shapes and motions. Snakes have been used for edge and curve detection, segmentation, shape modelling, and visual tracking. The recent book by Blake and Yuille [8] contains an excellent collection of papers on the theory and practice of deformable contours together with a large list of references to which which we refer the interested reader.

In this note, we consider a method based on the elegant approaches of Caselles *et al.* [10] and Malladi *et al.* [31]. In these papers, a level set curve evolution method is presented to solve the problem. Our idea is simply to note that both these approaches are based on Euclidean curve shortening evolution which in turn defines the gradient direction in which the Euclidean perimeter is shrinking as fast as possible. (See Section 2.) We therefore modify the active contour models of [10, 31] by multiplying the Euclidean arc-length by a function tailored to the features of interest to which we want to flow, and then writing down the resulting *gradient evolution equations.* Mathematically, this amounts to defining a new Riemannian metric in the plane tailored to the given image, and then computing the corresponding gradient flow. This leads to some new snake models which efficiently attract the given active contour to the features of interest (which basically lie at the bottom of a *potential well*). The method also allows us to naturally write down 3-D active surface models as well.

We now summarize the contents of this paper. In Section 2, we discuss some of the relevant facts from Euclidean curve shortening. In Section 3, we present our modification of the Euclidean arc-length and the resulting active contour models. In Section 4, we consider how these models may be extended to surfaces, i.e., for deformable surface (or 3-D contour) models. Next in Section 5, we consider the existence and uniqueness of the solutions of our models from a viscosity point of view. Finally in Sections 6 and 7, we work out some examples and draw our conclusions.

2 Euclidean Curve Shortening

The motivation for the equations underlying active geometric contours comes from *Euclidean curve shortening.* Therefore, in this section we will review the relevant curve evolution theory in the plane R^2.

Accordingly, for κ the curvature, and $\vec{\mathcal{N}}$ the inward unit normal, one considers families of plane curves evolving according to the *geometric heat equation*

$$\frac{\partial C}{\partial t} = \kappa \vec{\mathcal{N}}. \tag{1}$$

This equation has a number of properties which make it very useful in image processing, and in particular, the basis of a nonlinear scale-space for shape representation [1, 3, 24, 25, 32].

Indeed, (1) is the Euclidean curve shortening flow, in the sense that the Euclidean perimeter shrinks as quickly as possible when the curve evolves according to (1) [16, 17, 21]. Since, we will need a similar argument for the snake model we discuss in the next section, let us work out the details.

Let $C = C(p,t)$ be a smooth family of closed curves where t parametrizes the family and p the given curve, say $0 \leq p \leq 1$. (Note we assume that $C(0,t) = C(1,t)$ and similarly for the first derivatives.) Consider the length functional

$$L(t) := \int_0^1 \|\frac{\partial C}{\partial p}\| dp.$$

Then differentiating (taking the "first variation"), and using integration by parts, we see that

$$\begin{aligned} L'(t) &= \int_0^1 \frac{\langle \frac{\partial C}{\partial p}, \frac{\partial^2 C}{\partial p \partial t} \rangle}{\|\frac{\partial C}{\partial p}\|} dp \\ &= -\int_0^1 \langle \frac{\partial C}{\partial t}, \frac{1}{\|\frac{\partial C}{\partial p}\|} \frac{\partial}{\partial p} \left[\frac{\frac{\partial C}{\partial p}}{\|\frac{\partial C}{\partial p}\|} \right] \|\frac{\partial C}{\partial p}\| \rangle dp. \end{aligned}$$

(Note that we multiplied and divided by $\|\frac{\partial C}{\partial p}\|$ in the latter integral.) But noticing now that

$$\|\frac{\partial C}{\partial p}\| dp =: ds$$

is (Euclidean) arc-length, and using the definition of curvature, the last integral is

$$-\int_0^{L(t)} \langle \frac{\partial C}{\partial t}, \kappa \vec{\mathcal{N}} \rangle ds$$

that is, we see

$$L'(t) = -\int_0^{L(t)} \langle \frac{\partial C}{\partial t}, \kappa \vec{\mathcal{N}} \rangle ds.$$

Thus the direction in which $L(t)$ is decreasing most rapidly is when

$$\frac{\partial C}{\partial t} = \kappa \vec{\mathcal{N}}.$$

Thus (1) is precisely a gradient flow.

A much deeper fact is that simple closed curves converge to "round" points when evolving according to (1) without developing singularities; see [17, 21]. This fact is one of the keys for the geometric active contour models considered below.

3 Active Snake Model

In two remarkable papers, Caselles *et al.* [10] and Malladi *et al.* [31] propose a snake model based on the level set formulation of the Euclidean curve shortening equation. More precisely, their model is

$$\frac{\partial \Psi}{\partial t} = \phi(x,y)\|\nabla\Psi\|(\mathrm{div}(\frac{\nabla\Psi}{\|\nabla\Psi\|}) + \nu). \tag{2}$$

Here the function $\phi(x,y)$ depends on the given image and is used as a "stopping term." For example, the term $\phi(x,y)$ may chosen to be small near an edge, and so acts to stop the evolution when the contour gets close to an edge. In [10, 31], the term

$$\phi := \frac{1}{1+\|\nabla G_\sigma * I\|^2} \tag{3}$$

is chosen, where I is the (grey-scale) image and G_σ is a Gaussian (smoothing filter) filter. The function $\Psi(x,y,t)$ evolves in (2) according to the associated level set flow for planar curve evolution in the normal direction with speed a function of curvature which was introduced in the fundamental work of Osher-Sethian [37, 38, 44, 45, 46].

It is important to note that as we have seen above, the Euclidean curve shortening part of this evolution, namely

$$\frac{\partial \Psi}{\partial t} = \|\nabla\Psi\|\mathrm{div}(\frac{\nabla\Psi}{\|\nabla\Psi\|}) \tag{4}$$

is derived as a gradient flow for shrinking the perimeter as quickly as possible. As is explained in [10], the constant *inflation term* ν is added in (2) in order to keep the evolution moving in the proper direction. Note that we are taking Ψ to be negative in the interior and positive in the exterior of the zero level set.

Remarks 1.

1. In [31], the inflationary constant is considered both with a positive sign (inward evolution) and with a negative sign (outward or expanding evolution). (Note the sign convention we have taken for Ψ above.) In the latter case, this can be referred to as expanding "balloons." For simplicity, unless stated otherwise explicitly, we will take $\nu \geq 0$ (inward evolutions) in what follows below.

2. Instead of using a Gaussian to smooth the image one may of course use the a nonlinear smoothing filter based on the curvature; see [4].

We would like to modify the model (2) in a manner suggested by the computation in Section 2. Namely, we will change the ordinary Euclidean arc-length function along a curve $C = (x(p), y(p))^T$ with parameter p given by

$$ds = (x_p^2 + y_p^2)^{1/2} dp$$

to

$$ds_\phi = (x_p^2 + y_p^2)^{1/2} \phi dp,$$

where $\phi(x, y)$ is a positive differentiable function. We now essentially repeat the computation made in Section 2, i.e., we want to compute the corresponding gradient flow for shortening length relative to the new metric ds_ϕ.

Accordingly set

$$L_\phi(t) := \int_0^1 \|\frac{\partial C}{\partial p}\| \phi dp.$$

Let

$$\vec{\mathcal{T}} := \frac{\partial C}{\partial p} / \|\frac{\partial C}{\partial p}\|,$$

denote the unit tangent. Then taking the first variation of the modified length function L_ϕ, and using integration by parts just as above, we get that

$$L'_\phi(t) \;=\; \int_0^{L_\phi(t)} \langle \frac{\partial C}{\partial t}, \phi\kappa\vec{\mathcal{N}} + (\nabla\phi \cdot \vec{\mathcal{T}})\vec{\mathcal{T}} - \nabla\phi \rangle ds_\phi$$

which means that the direction in which the L_ϕ perimeter is shrinking as fast as possible is given by

$$\frac{\partial C}{\partial t} = \phi\kappa\vec{\mathcal{N}} + (\nabla\phi \cdot \vec{\mathcal{T}})\vec{\mathcal{T}} - \nabla\phi. \tag{5}$$

This is precisely the gradient flow corresponding to the miminization of the length functional L_ϕ. Since the tangential component of equation (5) may be dropped (see [15]), this may be simplified to

$$\frac{\partial C}{\partial t} = \phi\kappa\vec{\mathcal{N}} - \nabla\phi. \tag{6}$$

The level set version of this is

$$\frac{\partial \Psi}{\partial t} = \phi\|\nabla\Psi\| \mathrm{div}(\frac{\nabla\Psi}{\|\nabla\Psi\|}) + \nabla\phi \cdot \nabla\Psi. \tag{7}$$

One expects that this evolution should attract the contour very quickly to the feature which lies at the bottom of the *potential well* described by the gradient flow (7). As in [10, 31], we we may also add a constant inflation term, and so derive a modified model of (2) given by

$$\frac{\partial \Psi}{\partial t} = \phi\|\nabla\Psi\|(\mathrm{div}(\frac{\nabla\Psi}{\|\nabla\Psi\|}) + \nu) + \nabla\phi \cdot \nabla\Psi. \tag{8}$$

Notice that for ϕ as in (3), $\nabla\phi$ will look like a doublet near an edge. Of course, one may choose other candidates for ϕ in order to pick out other features.

We have implemented this snake model based on the algorithms of Osher-Sethian [37, 38, 44, 45, 46] and Malladi *et al.* [31]. We are also experimenting with some new code based on [35].

Remarks 2.

1. Note that the metric ds_ϕ has the property that it becomes small where ϕ is small and vice versa. Thus at such points lengths decrease and so one needs less "energy" in order to move. Consequently, it seems that such a metric is natural for attracting the deformable contour to an edge when ϕ has the form (3).

2. Kumar *et al.* [28] using a similar modification of the affine metric have developed an affine invariant snake model as well. In this case, the role of the function ϕ is played by an affine invariant edge detector developed in [28].

4 3-D Active Contour Models

In this section, we will discuss some possible geometric 3-D contour models based on surface evolution ideas, by modifying the Euclidean area in this case by a function which depends on the salient features which we wish to capture. In order to do this, we will need to set up some notation. (For all the relevant concepts on the differential geometry of surfaces, we refer the reader to [14].)

Let $S : [0,1] \times [0,1] \to R^3$ denote a compact embedded surface with (local) coordinates (u, v). Let H denote the mean curvature and $\vec{\mathcal{N}}$ the inward unit normal. We set

$$S_u := \frac{\partial S}{\partial u}, \quad S_v := \frac{\partial S}{\partial v}.$$

Then the infinitesimal area on S is given by

$$dS = (\|S_u\|^2\|S_v\|^2 - \langle S_u, S_v\rangle^2)^{1/2} du dv.$$

Let $\phi : \Omega \to R$ be a positive differentiable function defined on some open subset of R^3. The function $\phi(x, y, z)$ will play the role of the "stopping" function ϕ given above in our snake model (7, 8).

It is a beautiful classical fact that the gradient flow associated to the area functional for surfaces (i.e., the direction in which area is shrinking most rapidly) is given by

$$\frac{\partial S}{\partial t} = H\vec{\mathcal{N}}. \tag{9}$$

(See [9, 19, 33, 36, 52] and the references therein.) What we propose to do is to replace the Euclidean area by a modified area depending on ϕ namely,

$$dS_\phi := \phi dS.$$

For a family of surfaces (with parameter t), consider the ϕ-area functional

$$A_\phi(t) := \int\int_S dS_\phi.$$

Once again, an integration by parts argument gives that

$$\frac{dA_\phi}{dt} = -\int\int_S \langle \frac{\partial S}{\partial t}, \phi H\vec{\mathcal{N}} - \nabla\phi + \text{tangential components}\rangle dS,$$

which after dropping the tangential part becomes

$$\frac{\partial S}{\partial t} = \phi H\vec{\mathcal{N}} - \nabla\phi. \tag{10}$$

The level set version of (10) is given in terms of $\Psi(x, y, z, t)$ by

$$\Psi_t = \phi\|\nabla\Psi\|\text{div}(\frac{\nabla\Psi}{\|\nabla\Psi\|}) + \nabla\phi\cdot\nabla\Psi. \tag{11}$$

As before one may add a constant inflation term to the mean curvature to derive the model

$$\Psi_t = \phi\|\nabla\Psi\|(\text{div}(\frac{\nabla\Psi}{\|\nabla\Psi\|}) + \nu) + \nabla\phi\cdot\nabla\Psi. \tag{12}$$

In the context of image processing, the term ϕ depends on the given 3-D image and is exactly analogous to the stopping term in (7, 8). It is important to note that there is a very big difference between the 2-D and 3-D models discussed here. Indeed, the geometric heat equation will shrink a simple closed curve to a round point without developing singularities, even if the initial curve is *nonconvex*. The geometric model (2) is based on this flow. For surfaces, it is well-known that singularities may develop in the mean curvature flow (9) non-convex smooth surfaces [20]. (The classical example is the dumbbell.) We should note however that the mean curvature flow does indeed shrink smooth compact convex surfaces to round "spherical" points; see [23].

We should add that because of these problems, several researchers have proposed replacing mean curvature flow by flows which depend on the Gaussian curvature κ. Indeed, define

$$\kappa_+ := \max\{\kappa, 0\}.$$

Then Caselles and Sbert [11] have shown that the *affine invariant flow*

$$\frac{\partial S}{\partial t} = \text{sign}(H)\kappa_+^{1/4}\vec{\mathcal{N}} \tag{13}$$

will (smoothly) shrink rotationally symmetric compact surfaces to ellipsoidal shaped points. (This has been proven in [6] in the convex case. See also [2, 5].) Thus one could replace the mean curvature part by $\mathrm{sign}(H)\kappa_+^{1/4}$ in (12). Another possibility would be to use $\kappa_+^{1/2}$ as has been proposed in [34]. See also [51]. (Note that Chow [12] has shown that convex surfaces flowing under $\kappa^{1/2}$ shrink to spherical points.) All these possible evolutions for 3-D contours are now being explored.

5 Viscosity Analysis of the Models

In this section, we will outline the analysis of the nonlinear diffusion equation

$$\Psi_t = \phi(x)a^{ij}(\nabla\Psi)\partial_{ij}\Psi + H(x,\nabla\Psi), \quad x = (x_1,\ldots,x_n), \tag{14}$$

of which the models of Caselles *et al.* [10] and Malladi *et al.* [31], and the equations we study here are special cases. Note that we use the summation convention systematically in (14) and in what follows. This section is rather mathematically technical, and has been included to rigorously justify the partial differential equations we have been using. We use the standard notation from the theory of partial differential equations as may be found in [48].

Because of the form of a^{ij}, and the fact that ϕ may vanish, this problem requires some care; in particular, the solutions are not expected to be sufficiently regular for the equation to make sense, and we need to use a type of generalized solutions known as *viscosity solutions*, defined below. The technicalities are very similar to those in [4], [10].

In what follows, the letter C is used to denote various positive constants, the exact value of which is not significant. We assume that H is the sum of $-\nabla\Psi\cdot\nabla\phi$ and an "inflation term" $\nu\phi\|\nabla\Psi\|$. We also assume that ϕ and $\sqrt{\phi}$ are Lipschitz continuous. While ϕ and H are continuous in their arguments, a^{ij} is not:

$$a^{ij}(p) = \delta^{ij} - \frac{p_i p_j}{\|p\|^2}, \quad p = (p_1,\ldots,p_n).$$

Note that in the latter expression δ^{ij} denotes the Kronecker delta. We use periodic boundary conditions in the spatial domain, and consider a Lipschitz continuous initial value $\Psi_0(x)$. Our solutions will have bounded first derivatives, but will not have second-order derivatives in general.

Viscosity interpretation of equation (14):

Since the solution is not twice differentiable, we must use a notion of *weak solution.* Since the equation is not in the form of a divergence, the familiar integration by parts argument used for shock waves does not help.

We use the notion of "viscosity solution" which has proved useful in this context.

We first define sub- and super-solutions. A viscosity solution will be by definition any function which is both a sub-solution and a super-solution in the following sense.

A function f is said to be a *sub-solution* if f is defined and continuous for all x, and $0 \leq t \leq T$ for some $T > 0$, and is such that whenever g is a twice continuously differentiable function and $(f - g)$ attains a local maximum at a point (x_0, t_0) with $t_0 > 0$, one has

$$g_t(x_0, t_0) - \phi(x_0) a^{ij}(Dg(x_0, t_0)) \partial_{ij} g(x_0, t_0) - H(x_0, \nabla g(x_0, t_0)) \leq 0,$$

if $\nabla g(x_0, t_0) \neq 0$. If $\nabla g(x_0, t_0) = 0$, we require instead

$$g_t(x_0, t_0) - \phi(x_0) \limsup_{p \to 0} a^{ij}(p) \partial_{ij} g(x_0, t_0) - H(x_0, \nabla g(x_0, t_0)) \leq 0;$$

this latter form being made necessary by the fact the a^{ij} is not continuous for $p = 0$.

A *super-solution* is similarly defined, by requiring that $(f - g)$ have a local minimum, replacing lim sup by lim inf, and reversing the direction of all inequalities. As already mentioned, a *viscosity solution* is a continuous function which is both a sub- and a super-solution.

We can now state the following result:

Theorem 1 *There is a unique viscosity solution in* $L^\infty(0, T; W^{1,\infty}(R^n))$.

Proof. The construction of the solution proceeds by solving an approximate uniformly parabolic problem, and by passing to the limit. The uniqueness is more delicate and requires a lemma from Crandall-Ishii [13]; the outcome will be an estimate for the difference of two solutions with different initial data.

STEP 1: (Gradient bounds).
We consider here the case when the nonlinearities are all smooth. These considerations will apply to a regularized version of our equation. In the following, subscripts denote derivatives.

Let Ψ be a solution. Differentiation of the equation gives

$$\partial_t \Psi_k - \phi_k a^{ij} \Psi_{ij} - \phi \left[\frac{\partial a_{ij}}{\partial p^l} \Psi_{lk} \Psi_{ij} + a^{ij} \Psi_{ijk} \right] - \frac{\partial H}{\partial p_l} \Psi_{lk} - \frac{\partial H}{\partial x^k} = 0.$$

We multiply this equation by $2\Psi_k$ and sum over k to find:

$$M_t - \phi \left[a^{ij} \partial_{ij} M + \frac{\partial a_{ij}}{\partial p^l} \Psi_{ij} \partial_l M \right] + \frac{\partial H}{\partial p_l} M_l = -2\phi a^{ij} \Psi_{ik} \Psi_{jk} + 2\partial_k \phi \left[a^{ij} \Psi_{ij} \Psi_k + H \Psi_k \right],$$

where $M = \|\nabla \Psi\|^2$.

We now choose our approximation:

$$a^{ij}_\varepsilon + \varepsilon \delta^{ij} + \left(\delta^{ij} - \frac{p_i p_j}{\|p\|^2 + \varepsilon^2} \right).$$

We also replace $\|\nabla \Psi\|$ by $\sqrt{\|\nabla \Psi\|^2 + \varepsilon^2}$ in the inflation term.

Since we assumed that $\sqrt{\phi}$ is Lipschitz, we have

$$|\partial_k \phi| \leq C\sqrt{\phi}.$$

On the other hand, reducing the symmetric semi-definite matrix (a^{ij}) to its principal axes, it is easy to see that

$$(a^{ij}\Psi_{ij})^2 \leq C(a^{ij}\Psi_{ik}\Psi_{jk})$$

for some constant C. Combining these two estimates, we find that Since $H \leq C\|\nabla\Psi\|$, we find, using the maximum principle for uniformly parabolic equations, that

$$\|\nabla\Psi\|_{L^\infty}(t) \leq e^{Ct}(\|\nabla\Psi\|_{L^\infty}(0) + \varepsilon^2).$$

A global Lipschitz estimate in space for solutions of the approximate equation follows.

STEP 2: (Convergence of approximations).
The gradient bound in space implies in fact a Hölder estimate with exponent $1/2$ in time. We may therefore apply Ascoli's theorem to conclude that a solution exists. To prove its uniquness will require more sophisticated tools from the theory of viscosity solutions.

STEP 3: (Comparison principle and uniqueness).
Let two solutions Ψ_1 and Ψ_2 be given (both in the viscosity sense). We define

$$\alpha(x, y, t) = \Psi_1(t, x) - \Psi_2(y, t) - (4\varepsilon)^{-1}\|x - y\|^4 - \lambda t,$$

where λ is an arbitrary positive constant. We claim that on $0 \leq t \leq T$, this function is maximum for $t = 0$. Indeed, otherwise, the maximum would be attained at some point (x_0, y_0, t_0) with $t_0 > 0$. By a lemma of Crandall and Ishii [13], for any positive μ, there are real numbers a and b, and symmetric matrices X and Y such that

$$a - b = \lambda$$

and

$$\begin{pmatrix} X & 0 \\ 0 & -Y \end{pmatrix} \leq A + \mu A^2,$$

where

$$A = \begin{pmatrix} B & -B \\ -B & B \end{pmatrix},$$

with

$$B_{ij} = \varepsilon^{-1}\|x_0 - y_0\|^2\delta_{ij} + (2/\varepsilon)(x_0 - y_0)_i(x_0 - y_0)_j.$$

In addition, one has

$$a - \phi(x_0)a^{ij}(\varepsilon^{-1}\|x_0 - y_0\|^2(x_0 - y_0))X_{ij} - H(\varepsilon^{-1}\|x_0 - y_0\|^2(x_0 - y_0)) \leq 0$$

and

$$b - \phi(y_0)a^{ij}(\varepsilon^{-1}\|x_0 - y_0\|^2(x_0 - y_0))Y_{ij} - H(y_0, \varepsilon^{-1}\|x_0 - y_0\|^2(x_0 - y_0)) \geq 0.$$

If $x_0 = y_0$, these relations have to be interpreted in terms of a suitable limit, but this case leads to $a \leq 0 \leq b$, which contradicts the assumption $\lambda > 0$. So $x_0 \neq y_0$.

Next, choose $\mu = \varepsilon\|x_0 - y_0\|^{-2}$ (which is now possible), and conclude that

$$\begin{pmatrix} X & 0 \\ 0 & -Y \end{pmatrix} \leq \frac{2}{\varepsilon}\begin{pmatrix} D & -D \\ -D & D \end{pmatrix},$$

where

$$D_{ij} = \|x_0 - y_0\|^2\delta_{ij} + 5(x_0 - y_0)_i(x_0 - y_0)_j.$$

Multiplying this inequality by G, where

$$G = \begin{pmatrix} \phi(x_0)B & \sqrt{\phi(x_0)\phi(y_0)}B \\ \sqrt{\phi(x_0)\phi(y_0)}B & \phi(y_0)B \end{pmatrix},$$

and taking the trace, we obtain after some manipulation, using the fact that a^{ij} is bounded, the definition of a viscosity solution, and the fact that $\sqrt{\phi}$ is Lipschitz, an inequality

$$\lambda \leq C_0\|x_0 - y_0\|^4/\varepsilon.$$

Using the Lipschitz condition on the functions Ψ_1 and Ψ_2, and the property $\alpha(t_0, x_0, y_0) \geq \alpha(t_0, y_0, y_0)$, we derive a bound

$$\lambda \leq C\varepsilon^{1/3}L^{4/3}.$$

Taking

$$\varepsilon^{1/3} = \delta K$$

and

$$\lambda = 2C_0\delta K L^{4/3},$$

with $K = \sup_{[0,T]\times R^n}|\Psi_1 - \Psi_2|$, we find that the bound on λ leads to an absurdity. We therefore can conclude that $t_0 = 0$.

We fix λ and ε as before. Using $t_0 = 0$, we find that

$$\sup_{[0,T]\times R^n} |\Psi_1 - \Psi_2| \leq \sup_{R^n} |\Psi_1 - \Psi_2|(0) + \frac{3}{4}\delta K L^{4/3} + 2C_0 \delta K L^{4/3} T.$$

Letting $\delta \to 0$, we finally obtain

$$\sup_{[0,T]\times R^n} |\Psi_1 - \Psi_2| \leq \sup_{R^n} |\Psi_1 - \Psi_2|(0),$$

which proves uniqueness and stability with respect to initial conditions. □

We can conclude from Theorem 1 that slight differences between images will not become artificially enhanced by our active contour methods.

6 Experiments

We will now give a few numerical experiments to illustrate our methods. Full details about the numerics will appear elsewhere as well as applications to more realistic MRI and ultrasound medical imagery. The implementations we have used are based on the level set evolution methods developed by Osher-Sethian [37, 38, 44, 45, 46], and the techniques in [31].

The equations described in this paper have been coded for the case of active contours on two-dimensional images. The code is still in an early form and work is in progress to improve various aspects of it. We will present here some preliminary experimental results obtained by running this code on both binary (i.e., high contrast images) and real images. At this stage of the work the images have been selected purely for the purposes of illustration. The images are sampled at discrete pixel locations as usual.

6.1 Numerical Aspects of Level Set Evolution

For 2D active contours, the evolution equation as derived in Section 3 is equation (8),

$$\frac{\partial \Psi}{\partial t} = \phi \|\nabla \Psi\| (\mathrm{div}(\frac{\nabla \Psi}{\|\nabla \Psi\|}) + \nu) + \nabla \phi \cdot \nabla \Psi,$$

where ν is a constant inflation force and $\kappa := \mathrm{div}(\frac{\nabla \Psi}{\|\nabla \Psi\|})$ is the curvature of the level sets of $\Psi(x, y, t)$. This equation describes a propagating front, and we are interested in its propagation in the plane of an image. It is known that a propagating front may not remain smooth at all times (for example, it may cross itself). For evolution beyond the discontinuities the solutions are required to satisfy an entropy condition to ensure that the front remains physically meaningful at all times. The discrete approximations to the spatial derivatives are thus

derived from the entropy condition. Osher-Sethian [38] have given such entropy satisfying schemes and these have been used successfully in shape modelling [31]. Following [31] we can regard a decomposition of our speed function as,

$$F(\kappa) = \nu + \mathrm{div}(\frac{\nabla\Psi}{\|\nabla\Psi\|}) = \nu + \kappa, \tag{15}$$

where ν is regarded as the constant passive advection term and the curvature κ is the diffusive term of the speed function. The inflation part in equation (8), i.e., $\nu\phi\|\nabla\Psi\|$ is approximated using upwind schemes. The diffusive part, i.e., $\kappa\phi\|\nabla\Psi\|$ is approximated using usual central differences. For the inner product term $\nabla\phi \cdot \nabla\Psi$, we use a certain thresholding smoothing method for the "doublet" $\nabla\phi$ which will be described in full detail in the journal version of this paper.

As discussed in [31], an important aspect of the propagation as given in equation (8) is that the image-based terms only have meaning on the zero-level set. Thus these terms must be extended to all the level sets to get a globally defined *extension*. To do this, we have basically followed the methods reported in [31] to which we refer the reader for all the details.

There are also stability implications of the choice of the step sizes, and in [31] it is noted that for the evolution equation used in that work the requirement is $\Delta t = O(\Delta x^2)$. Therefore if small spatial step sizes are used, it forces a small time step and the resulting evolution can be very slow. One way to speed up the evolution is to use a larger inflationary force and move the front faster (recall the advection term causes a constant contraction/expansion of the front). However, in our experience with using the approach in [31] this results in large motion of the front causing "overshooting" of the edge of the feature of interest in the image. This problem is resolved by the evolution in equation (8). $\nabla\phi$ has a behavior similar to a doublet near an edge. Thus, it exerts a "stronger" stopping effect and arrests the evolution of the contour close to an edge. In our experiments we have observed that this arresting behavior of the $\nabla\phi \cdot \nabla\Psi$ term allows use of large inflationary forces, resulting in features being extracted in relatively fewer time steps. In fact, the behavior of the inner product term is much more interesting, but we leave that for discussion in the full journal version of this note.

6.2 Image Feature Extraction Results

Here we sketch a few experimental results obtained using the feature extraction algorithm developed in this paper based on equation (8). First we present the result of feature extraction on a synthetic high contrast image consisting of three shapes. The image is a 150 x 150 binary image with intensity values 0 or 255. The entire image is used in the computations. Figure 1(a) shows the image with the initial contour. The time step used was $\Delta t = 0.000001$

and Figures 1(b) through 1(d) show the evolving contour at intermediate time steps. Figure 1(d) corresponds to 400 iterations.

In Figure 2, we present a convoluted shape to be extracted using an active contour. The image is a 150 x 150 binary image with binary intensity values as before. The entire image was used in the computations. Figure 2(a) shows the initial contour. Figures 2(b) through 2(f) show the evolving contour at 200, 400, 600, 800, and 1000 iterations. The shape of the feature has been completely captured by 1000 iterations. Again the time step used was $\Delta t = 0.000001$.

Finally, we present the result of evolution of an active contour in a real image. The aim of this experiment was to demonstrate the ability of the active contour in capturing the finer features in real images and also the abililty to capture more than one feature. The image is a 256 x 240 gray-scale image of a Rubik's cube placed on a circular table with a pattern on the table's side. An initial contour is placed with the aim of capturing the cube, the edge of the table and also the patterns on the side of the table. Figure 4(a) shows the intial contour. Figures 4(b) through 4(d) show the evolving contour after 100, 200, and 300 iterations. The time step used was $\Delta t = 0.001$. After 200 iterations the contour has captured the Rubik's cube and the table's edge. At 300 iterations most of the patterns we wished to capture on the table's side have been obtained. Indeed, the active contour finds the edge of the table from both the inside and the outside as well as the Rubik's cube itself. Notice that the snake also captures the shadow of the cube.

7 Conclusions

In this note, we have considered possible modifications of the active contour models based on those of [10, 31]. The basic concept is that we consider snakes in the framework of gradient flows relative to modified arc-length functionals. The active contour therefore flows to the desired feature regarded as lying at the bottom of the corresponding potential energy well. Possible 3-D surface models were also proposed using these energy ideas. We also presented a viscosity justification of our models as well as some illustrative numerical examples. Finally, this type of method may be extended to a number of different metrics, e.g., the affine metric in [28].

Acknowledgements: We would first like to thank Professor Tryphon Georgiou of the University of Minnesota for a number of very helpful conversations. This work was supported in part by grants from the National Science Foundation DMS-8811084, ECS-9122106, by the Air Force Office of Scientific Research F49620-94-1-00S8DEF, by the Army Research Office DAAH04-94-G-0054 and DAAH04-93-G-0332, and by Image Evolutions Limited.

References

[1] L. Alvarez, F. Guichard, P. L. Lions, and J. M. Morel, "Axiomes et equations fondamentales du traitement d'images," *C. R. Acad. Sci. Paris*, 315:135–138, 1992.

[2] L. Alvarez, F. Guichard, P. L. Lions, and J. M. Morel, "Axioms and fundamental equations of image processing," Report #9216, CEREMADE, Université Paris Dauphine, 1992.

[3] L. Alvarez, F. Guichard, P. L. Lions, and J. M. Morel, "Axiomatisation et nouveaux operateurs de la morphologie mathematique," *C. R. Acad. Sci. Paris* 315:265–268, 1992.

[4] L. Alvarez, P. L. Lions, and J. M. Morel, "Image selective smoothing and edge detection by nonlinear diffusion," *SIAM J. Numer. Anal.* **29**, pp. 845-866, 1992.

[5] L. Alvarez and J. M. Morel, "Formalization and computational aspects of image analysis," Report #0493, Department of Information and Systems, Universidad de las Palmas de Gran Canaria, 1993.

[6] B. Andrews, "Contraction of convex hypersurfaces by their affine normal," submitted for publication, 1994.

[7] S. Angenent, "On the formation of singularities in the curve shortening flow," *J. Differential Geometry* **33**, pp. 601-633, 1991.

[8] A. Blake and A. Yuille, *Active Vision*, MIT Press, Cambridge, Mass., 1992.

[9] K. A. Brakke, *The Motion of a Surface by its Mean Curvature*, "Princeton University Press, Princeton, NJ, 1978.

[10] V. Caselles, F. Catte, T. Coll, and F. Dibos, "A geometric model for active contours in image processing," Technical Report #9210, CEREMADE, Université Paris Dauphine, 1992.

[11] V. Caselles and C. Sbert, "What is the best causal scale-space for 3D images?," Technical Report, Department of Math. and Comp. Sciences, University of Illes Balears, 07071 Palma de Mallorca, Spain, March 1994.

[12] B. Chow, "Deforming convex hypersurfaces by the nth root of the Gaussian curvature," *J. Differential Geometry* **22**, pp. 117-138, 1985.

[13] M. G. Crandall and H. Ishii, "The maximum principle for semicontinuous functions," *Diff. and Integral Eqs.* **3**, pp. 1001-1014, 1990.

[14] M. P. Do Carmo, *Differential Geometry of Curves and Surfaces*, Prentice-Hall, Inc., New Jersey, 1976.

[15] C. L. Epstein and M. Gage, "The curve shortening flow," in *Wave Motion: Theory, Modeling, and Computation*, A. Chorin and A. Majda, Editors, Springer-Verlag, New York, 1987.

[16] M. Gage, "Curve shortening makes convex curves circular," *Invent. Math.* **76**, pp. 357-364, 1984.

[17] M. Gage and R. S. Hamilton, "The heat equation shrinking convex plane curves," *J. Differential Geometry* **23**, pp. 69-96, 1986.

[18] I. M. Gelfand and S. V. Fomin, *Calculus of Variations*, Prentice-Hall, Englewood Cliffs, N. J., 1963.

[19] C. Gerhardt, "Flow of nonconvex hypersurfaces into spheres," *J. Differential Geometry* **32**, pp. 299-314, 1990.

[20] M. Grayson, "A short note on the evolution of a surface by its mean curvature," *Duke Math. Journal* **58**, pp. 555-558, 1989.

[21] M. Grayson, "The heat equation shrinks embedded plane curves to round points," *J. Differential Geometry* **26**, pp. 285-314, 1987.

[22] M. Grayson, "Shortening embedded curves," *Annals of Mathematics* **129**, pp. 71-111, 1989.

[23] G. Huisken, "Flow by mean curvature of convex surfaces into spheres," *J. Differential Geometry* **20**, pp. 237-266, 1984.

[24] B. B. Kimia, A. Tannenbaum, and S. W. Zucker, "Toward a computational theory of shape: An overview", *Lecture Notes in Computer Science* **427**, pp. 402-407, Springer-Verlag, New York, 1990.

[25] B. B. Kimia, A. Tannenbaum, and S. W. Zucker, "Shapes, shocks, and deformations, I," to appear in *Int. J. Computer Vision.*

[26] B. B. Kimia, A. Tannenbaum, and S. W. Zucker, "On the evolution of curves via a function of curvature, I: the classical case," *J. of Math. Analysis and Applications* **163**, pp. 438-458, 1992.

[27] A. Kumar, *Visual Information in a Feedback Loop*, Ph. D. thesis, University of Minnesota, 1995.

[28] A. Kumar, P. Olver, G. Sapiro, and A. Tannenbaum, "On an affine invariant active contour model," in preparation.

[29] R. J. LeVeque, *Numerical Methods for Conservation Laws*, Birkhäuser, Boston, 1992.

[30] P. L. Lions, *Generalized Solutions of Hamilton-Jacobi Equations*, Pitman Publishing, Boston, 1982.

[31] R. Malladi, J. Sethian, and B. Vemuri, *Shape modeling with front propagation: a level set approach,* to appear in *IEEE Trans. Pattern Anal. Machine Intell.*

[32] F. Mokhatarian and A. Mackworth, "A theory of multiscale, curvature-based shape representation for planar curves," *IEEE Trans. Pattern Anal. Machine Intell.* **14**, pp. 789-805, 1992.

[33] F. Morgan, *Riemannian Geometry*, John and Bartlett Publishers, Boston, 1993.

[34] P. Neskovic and B. Kimia, "Three-dimensional shape representation from curvature-dependent deformations," Technical Report #128, LEMS, Brown University, 1994.

[35] R. H. Nochetto, M. Paolini, and C. Verdi "A dynamic mesh method algorithm for curvature dependent evolving interfaces," Technical Report, University of Maryland, 1994.

[36] P. Olver, G. Sapiro, and A. Tannenbaum, "Geomtric invariant evolution of surfaces and volumetric smoothing," submitted for publication in *SIAM J. Math. Anal.*, 1994.

[37] S. Osher, "Riemann solvers, the entropy condition, and difference approximations," *SIAM J. Numer. Anal.* **21**, pp. 217-235, 1984.

[38] S. J. Osher and J. A. Sethian, "Fronts propagation with curvature dependent speed: Algorithms based on Hamilton-Jacobi formulations," *Journal of Computational Physics* **79**, pp. 12-49, 1988.

[39] S. Osher and L. I. Rudin, "Feature-oriented image enhancement using shock filters," *SIAM J. Numer. Anal.* **27**, pp. 919-940, 1990.

[40] P. Perona and J. Malik, "Scale-space and edge detection using anisotropic diffusion," *IEEE Trans. Pattern Anal. Machine Intell.* **12**, pp. 629-639, 1990.

[41] M. H. Protter and H. F. Weinberger, *Maximum Principles in Differential Equations,* Springer-Verlag, New York, 1984.

[42] G. Sapiro and A. Tannenbaum, "Affine invariant scale-space," *International Journal of Computer Vision* **11**, pp. 25-44, 1993.

[43] G. Sapiro and A. Tannenbaum, "On invariant curve evolution and image analysis," *Indiana Univ. Journal of Math.* **42**, 1993.

[44] J. A. Sethian, *An Analysis of Flame Propagation*, Ph. D. Dissertation, University of California, 1982.

[45] J. A. Sethian, "Curvature and the evolution of fronts," *Commun. Math. Phys.* **101**, pp. 487-499, 1985

[46] J. A. Sethian, "A review of recent numerical algorithms for hypersurfaces moving with curvature dependent speed," *J. Differential Geometry* **31**, pp. 131-161, 1989.

[47] J. A. Sethian and J. Strain, "Crystal growth and dendritic solidification," *Journal of Computational Physics* **98**, 1992.

[48] J. Smoller, *Shock Waves and Reaction-diffusion Equations*, Springer-Verlag, New York, 1983.

[49] G. A. Sod, *Numerical Methods in Fluid Dynamics*, Cambridge University Press, Cambridge, 1985

[50] M. Spivak, *A Comprehensive Introduction to Differential Geometry*, Publish or Perish Inc, Berkeley, California, 1979.

[51] H. Tek and B. Kimia, "Deformable bubbles in the reaction-diffusion space," Technical Report #138, LEMS, Brown University, 1994.

[52] B. White, "Some recent developments in differential geometry," *Mathematical Intelligencer* **11**, pp. 41-47, 1989.

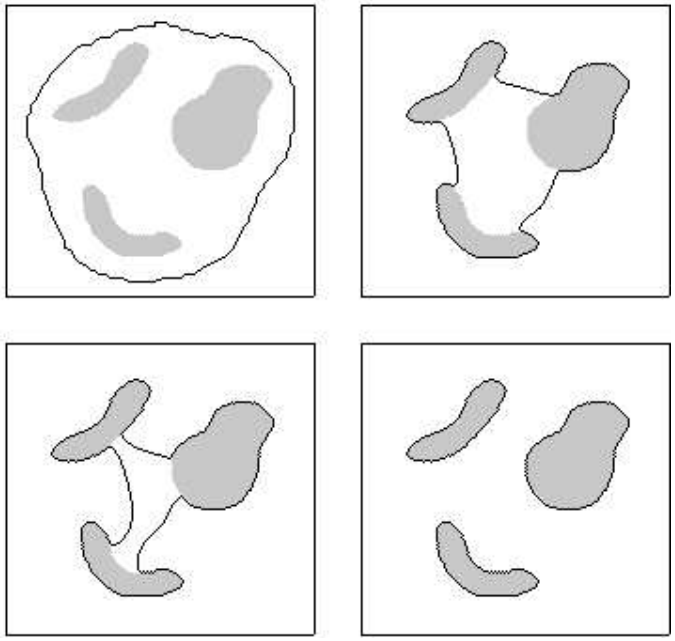

Figure 1: Feature extraction in a synthetic image. Left to right, top to bottom: (a) Initial contour. (b),(c),and (d) contour after 200, 300, and 400 iterations. $\Delta t = 0.000001$.

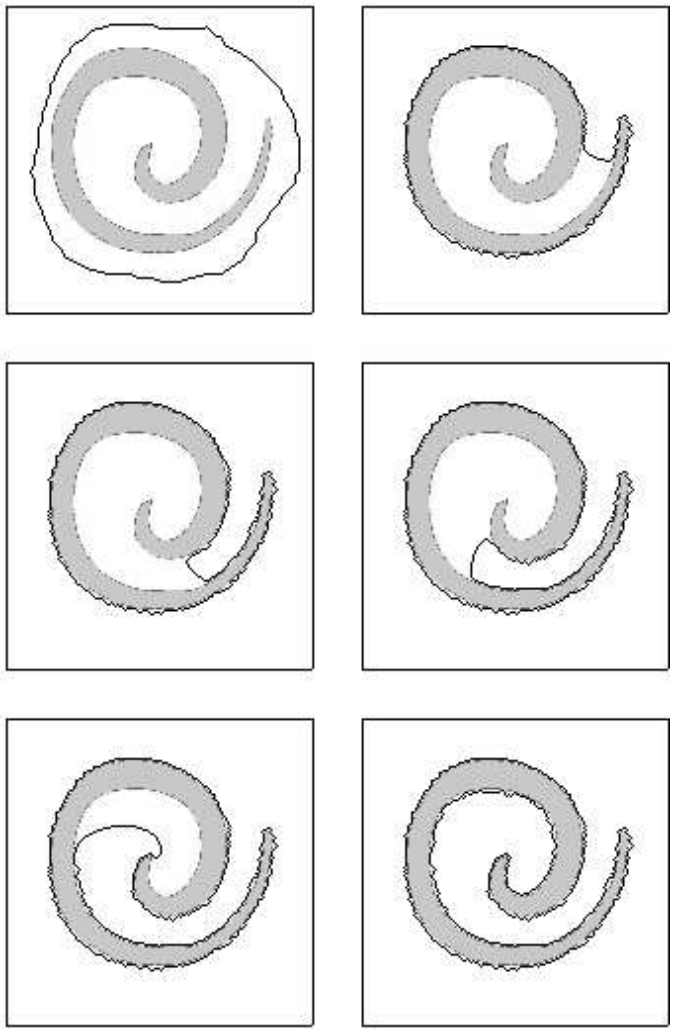

Figure 2: Feature extraction in a synthetic image. Left to right, top to bottom: (a) Initial contour. (b),(c),(d),(e),and (f) contour after 200, 400, 600, 800 and 1000 iterations. $\Delta t = 0.000001$.

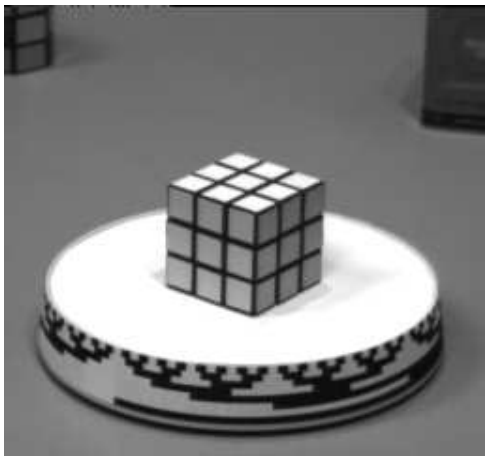

Figure 3: Rubik's Cube on a turntable.

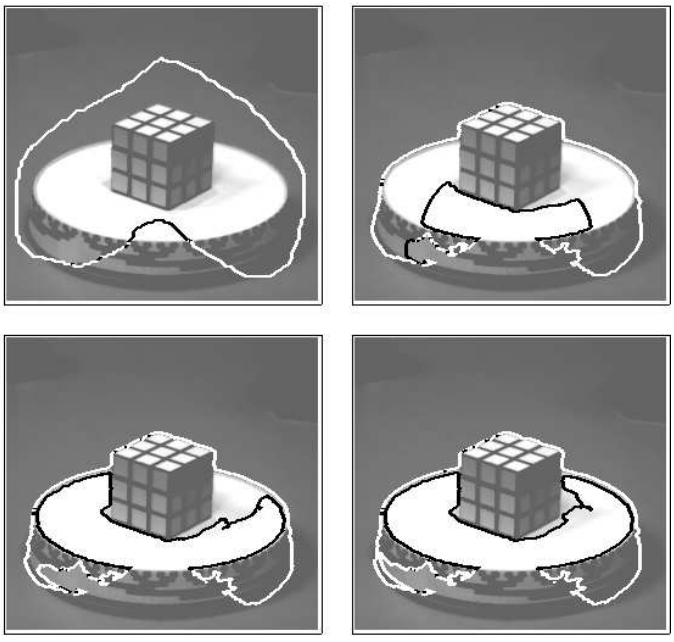

Figure 4: Feature extraction in a real image. Left to right, top to bottom: (a) Initial contour. (b),(c),and (d) contour after 100, 200, and 300 iterations. $\Delta t = 0.001$.